Separation and Purification Technology 310 (2023) 123193

Contents lists available at ScienceDirect

Separation and Purification Technology

journal homepage: www.elsevier.com/locate/seppur

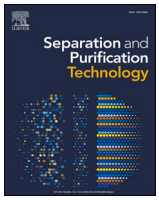

Alginate coated superparamagnetic iron oxide nanoparticles as nanocomposite adsorbents for arsenic removal from aqueous solutions

Somayeh Asadi Haris [a], Shadab Dabagh [a], Hamidreza Mollasalehi [b], Yavuz Nuri Ertas [a,c,*]

[a] ERNAM—Nanotechnology Research and Application Center, Erciyes University, Kayseri 38039, Turkey
[b] Department of Microbiology and Microbial Biotechnology, Faculty of Life Sciences and Biotechnology, Shahid Beheshti University, Tehran 1983969411, Iran
[c] Department of Biomedical Engineering, Erciyes University, Kayseri 38039, Turkey

ARTICLE INFO

Keywords:
Superparamagnetic iron oxide nanoparticles
Alginate beads
Adsorption
Wastewater
Arsenic

ABSTRACT

Superparamagnetic iron oxide nanoparticles (SPIONs) were synthesized by the hydrothermal method and used for effective removal of arsenite, As(III), in their native and alginate beads-encapsulated (SPIONs-Alg) forms. The size of SPIONs was determined as ~25 nm, and the structural properties of the adsorbents were validated using FTIR and XRD. The magnetization curve had zero coercivity, indicating superparamagnetism. Furthermore, the effects of pH, contact time, temperature, adsorbent dosage, and initial As(III) concentration on removal efficiency were studied. The optimum removal percentages for SPIONs and SPIONs-Alg were 99% and 90%, respectively, at pH 7, 30 °C, and 6.5 mg/L As (III) concentration. The Langmuir isotherm model ($R^2 \geq 0.97$ for SPIONs and $R^2 \geq 0.99$ for SPIONs-Alg) fitted the equilibrium data better than Freundlich. The As(III) adsorption capacity of sorbents was evaluated using the Langmuir adsorption isotherm and found to be 11.89 mg/g and 240.081 mg/g for SPIONs and SPIONs-Alg, respectively. The adsorption kinetic data for both adsorbents showed a better fit to the pseudo-second-order kinetic model ($R^2 \geq 0.99$). The spontaneity of the adsorption process, the endothermic nature of the sorption reaction, and the adsorbents' affinity for As(III) were determined using the negative ΔG, positive ΔH and ΔS values. SPIONs-Alg (1.5 g/l solid-to-liquid S/L ratio) could be collected easily, recovered using 0.1 M NaOH, and reused for five times (sorption ≥ 97%). The feasibility of SPIONs-Alg as a promising adsorbent for removing As(III) from wastewater is clearly validated.

1. Introduction

Increasing heavy metal concentrations in the environment remains a global challenge [1]. These materials may reach natural streams through the discharge of wastewater from industrial and human activities [2]. Water is one of the most essential human resources, with global economic, social, political, and environmental importance [3,4]. Water pollution as a result of rising population and manufacturing activity is one of the biggest concerns for scientists to manage since millions of people are being exposed to high levels of toxic metals through the consumption of contaminated drinking water [5]. International organizations such as the WHO (World Health Organization) study and assess the existence of these heavy metals and their impact on human health on a regular basis [5]. The most hazardous heavy metals, according to the United States Environmental Protection Agency (EPA), are arsenic, chromium, mercury, cadmium and lead [6]. Out of these toxic metals, arsenic has been determined to have the most negative impact on human health when consumed through drinking water contaminated with arsenic [7]. Both human activity (mine wastes, chemical pesticides, petroleum refining, and ceramic manufacturing enterprises) and natural processes (weathering, soil erosion, and volcanic emissions) can cause arsenic pollution of water [8]. Both the WHO and EPA have reduced the arsenic threshold limits for drinking water from 50 μg/L to 10 μg/L due to the deadly health effects produced by drinking arsenic-contaminated water [6,7]. Arsenic is found in the environment both in inorganic and organic forms (methyl and dimethyl arsenic compounds). Arsenite, As(III) (H_3AsO_3, $H_2AsO_3^-$, and $HAsO_3^{2-}$), and arsenate, As(V) (H_3AsO_4, $H_2AsO_4^-$, and $HAsO_4^{2-}$), are two inorganic forms of arsenic that are much more toxic than organic forms [9,10]. Arsenite is 20–60 times more toxic than arsenate while also being more mobile and thermodynamically stable. As(III) is also linked to a number of diseases, including skin, lung, liver, kidney, and bladder cancer, as

* Corresponding author at: ERNAM—Nanotechnology Research and Application Center, Department of Biomedical Engineering, Erciyes University, Kayseri 38039, Turkey.
E-mail address: yavuzertas@erciyes.edu.tr (Y.N. Ertas).

https://doi.org/10.1016/j.seppur.2023.123193
Received 16 December 2022; Received in revised form 8 January 2023; Accepted 12 January 2023
Available online 16 January 2023

well as cardiovascular and neurological effects [11–13]. Researchers have become more interested in studying arsenic pollution and methods for its removal as a result of growing evidence that arsenic can cause cancer in developing nations [1,5].

So far, several technologies have been developed to remove arsenic from water and wastewater, including membrane technologies [14,15], chemical precipitation [16], ion exchange [17], reverse osmosis [18], coagulation–flocculation [19], and electrochemical treatment [20]. These methods are generally ineffective at removing As(III). Adsorption, on the other hand, has demonstrated high As(III) and As(V) removal efficiencies [21,22]. Adsorption has many advantages, such as being simple to operate, having the potential for regeneration, and requiring less energy, water, and chemicals. This simple and cheap method would have a minimal environmental effect and be a viable option in developing nations where access to huge amounts of energy and financial resources might be difficult. Adsorption's mechanistic process allows for a wide range of adsorbent design and application [23,24]. Numerous adsorbents have been studied for As removal, such as sandy soils [25], activated carbon [24,26–29], activated alumina [30,31], hydrous zirconium oxide [32,33], lanthanum-loaded silica gel [34], metal-loaded coral limestone [35], titanium oxides [36], and metal oxides (hematite, magnetite, goethite, and ferrites) [37–43]. Among the innovative adsorbents, ferrite nanoparticles have received a great deal of attention due to their high surface area and highly active surface sites, which may lead to superior adsorption capacity and selective removal of specific pollutants [44]. Among them, spinel ferrite nanoparticles are frequently referred to as having a particularly significant potential for arsenic adsorption due to their unique advantages of magnetic and chemical stability [45]. The general formula of spinel ferrite nanoparticles is MFe_2O_4, where M represents various metal cations (M = Fe^{2+}, Mn^{2+}, Co^{2+}, Zn^{2+}, etc.) situated at a tetrahedral site and Fe situated at an octahedral site. Spinel ferrites' physical and chemical properties are determined by the type of M cation and by the distribution of both M and Fe^{3+} cations across tetrahedral and octahedral sites [46,47]. Spinel ferrites are classified as normal, inverse, or mixed based on the position of M(II) and Fe(III) site preferences. M(II) is found at tetrahedral sites, while Fe(III) is found at octahedral sites (e.g., Zn Fe_2O_4). In the inverse type, Fe(III) is equally distributed at both sites, whereas M(II) is equally distributed at only the octahedral sites (e.g., Fe_3O_4 and $CoFe_2O_4$). In a mixed spinel structure of ferrite, both ions randomly occupy the tetrahedral and octahedral sites (e.g., $MnFe_2O_4$) [48]. Any adsorbent's specific surface area increases with decreasing particle size, so this greater surface area results in a higher removal rate. Previous research has found that shrinking ferrite nanoparticles improves As(III) removal efficiency [46]. However, separation from treated water is challenging due to their nanoscale size. Magnetic separation has been shown to be more efficient and selective than traditional methods such as centrifugation or filtration for separating nanomaterials from aqueous environments [49]. Superparamagnetic iron oxide nanoparticles (SPIONs) have been used for the treatment of arsenic-polluted water [50]. Previous studies have demonstrated the superparamagnetic behavior of manganese ferrite nanoparticles ($MnFe_2O_4$ NPs), magnesium ferrite nanoparticles ($Mg_{0.27}Fe_{2.50}O_4$ NPs) and $Mg_xMn_{1-x}Fe_2O_4$ have proved in previous works [50–52].

Furthermore, regeneration and reuse of adsorbents can minimize the total cost of the removal process, which is crucial for low-income and developing nations. Because of the high reactivity and nanoscale size of ferrite nanoparticles, regeneration and reuse by traditional methods are generally difficult [53]. Additionally, the discharge of materials into treated water has the potential to damage natural flora and fauna. To resolve these problems, support materials were employed to immobilize ferrite nanoparticle adsorbents [54]. Immobilization of nanoparticles onto supports such as polystyrene anion exchangers, chitosan beads, and alginate beads has been reported to be highly effective at improving adsorption and reusability of adsorbents [55–59]. Recently, alginate beads have been widely being used in metal removal due to their favorable properties like high adsorption capacity, high water permeability, selectivity, biocompatibility, and biodegradability. Alginate is a polymer that is widely derived from brown algae and certain microorganisms [8]. According to earlier research, various metals may be removed from aqueous solutions using ferrite nanoparticle adsorbents enclosed in alginate beads [53,57,60,61]. Several studies reported that $MnFe_2O_4$ NPs have a high arsenic removal efficiency [62–64]. The superparamagnetic Mg-$MnFe_2O_4$ nanoparticles encapsulated in alginate have not been reported before. The preparation of this adsorbent was as economical and facile method under standard environmental conditions. Combining the unique properties of SPIONs and alginate can increase their efficiency where the suitable magnetization and high surface area of SPIONs lead to easy magnetic separation and superior adsorption capacity. And also, alginate beads, because of their appropriate features such as selectivity, biocompatibility, and high adsorption capacity, avoid the discharge of materials into treated water and can be easily reused.

Thus, in this study, superparamagnetic iron oxide nanoparticles encased in alginate beads (SPIONs-Alg) were produced and employed as adsorbents to treat an aqueous solution containing As (III). Kinetics, isotherm sorption studies, and the effects of contact time, starting adsorbate concentration, and pH were investigated. In addition to adsorption capacity, regeneration qualities that have never been reported by researchers, were examined. This innovative nanoadsorbent, if further developed, might enable a straightforward, one-step As(III) adsorption technique from water, without the pre- and post-treatments which are now required in industry.

2. Experimental

2.1. Materials

Magnesium(II) nitrate hexahydrate $Mg(NO_3)_2{\cdot}6H_2O$ (99.9%), manganese(II) nitrate $Mn(NO_3)_2{\cdot}6H_2O$ (99.9%), iron(III) nitrate nonahydrate $Fe(NO_3)_3{\cdot}9H_2O$ (99.9%), sodium arsenite ($NaAsO_2$), sodium alginate ($C_6H_9NaO_7$), and $CaCl_2{\cdot}2H_2O$ were obtained from Acros Organics (Morris Plains, NJ) and were procured from Merck and used without further purification. Sodium hydroxide (NaOH) and hydrochloric acid (HCl) were obtained from Sigma Aldrich. 0.1732 g of analytical grade $NaAsO_2$ was dissolved in 100 mL of double-distilled water to make a (1000 mg/L) stock solution of As(III). Moreover, the quantities of the nitrates are calculated according to their atomic/molecular weights too.

3. Synthesis of SPIONs

To formulate SPIONs ($Mg_{1-x}Mn_xFe_2O_4$), the hydrothermal method was used, where the greatest outcomes occurred at the value x = 0.5 ($Mg_{0.5}Mn_{0.5}Fe_2O_4$) (~8 nm) [51]. The hydrothermal reactions were conducted at autogenous pressure in a stainless-steel autoclave with a Teflon liner (63 mL total capacity). In a typical synthesis, the nitrate solution mixture was progressively mixed and transferred to an autoclave, and then 10 mL of an 8 M NaOH solution was added dropwise to the above solution while magnetic stirring was going on. The autoclave was sealed and maintained at 180 °C for 10 h. After the reaction was finished, the solid products were collected and dried in a vacuum oven at 90 °C for 5 h [65].

3.1. Synthesis of SPIONs-alginate beads

The synthesized SPIONs were immobilized by entrapping NPs in alginate matrix formed by ionic polymerization in $CaCl_2$ solution, in proportion to the following steps [57]. Briefly, 100 mL of the alginate gel matrix (3% wt) was prepared. Then, a suspension of SPIONs in 1:10 ratio was added into the matrix, and final volume of the mixture was adjusted to 150 mL by adding double-distilled water. The mixture was uniformly

mixed with a magnetic stirrer at a temperature of 50 °C for 6 h. Therefore, the mixture containing sodium alginate and NPs in a ratio of 9:1 (3 g alginate/0.34 g NPs) was formulated for 10% wt absorbent loading. Later, using the syringe-method, the suspension was extruded drop wise to calcium chloride bath (4%, w/v) 4 °C, and beads were produced through crosslinking of sodium alginate with $CaCl_2$ solution [63]. The beads were allowed to polymerize for 6 h, then removed from the solution by filtration and washed multiple times with double-distilled water to remove water-soluble chemicals, and air-dried for 48 h [66]. Fig. 1 shows the schematic diagram for the preparation procedure followed for the SPIONs and SPIONs-Alg.

3.2. Characterization

The synthesized SPIONs were physiochemically characterized for surface morphology, elemental composition, functional groups, particle size, and crystal structure using standard procedures [67]. The morphology of samples was analyzed by field emission scanning electron microscopy with energy dispersive X-ray spectroscopy (FESEM-EDX). The samples were subjected to characterization using X-ray diffraction (XRD) and a vibrating sample magnetometer (VSM Lakeshore 7304). The specific surface area of prepared samples was measured by Surface Area Analyzer (BELSORP mini II) using N_2 sorption method and the Brunauer–Emmett–Teller (BET) model. The Zeta potential was measured by Electrophoretic light scattering measurements using Malvern Zetasizer Nano ZS90. To define the functional groups existing on the surface of the adsorbent, Fourier transform infrared spectroscopy (FTIR, NEXUS 670, Nicolet, USA) via the KBr method (the range is from 400 to 4000 cm^{-1}) was used.

3.3. Adsorption experiments

Batch adsorption experiments were carried out to evaluate the removal efficiency of As(III) ions from aqueous solution by SPIONs and SPIONs-Alg [68]. Both adsorbents were separately incubated in 100-mL flasks containing As(III) solution and shaken at 150 rpm for 0–180 min on a temperature-controlled (10–50 °C) shaker to determine the optimum temperature and contact time [69]. The effects of pH (2–9) and initial As(III) concentration (0–7.5 mg/L) on the adsorption capacity of various adsorbents were investigated. By adding HCl for an acidic solution or NaOH for an alkaline solution, the initial pH was adjusted [70]. After incubation, adsorbents were periodically removed, powders were centrifuged, and beads were filtered, and the As(III) concentration in the remaining solution (supernatant) was determined using the modified molybdenum blue method [71]. Samples were filtered, dried, and stored at 4 °C for future analysis. The adsorption capacity (Q_e) and removal percentage (R%) of As(III) at the equilibrium were calculated as follows:

$$Q_e = \frac{(C_i - C_f)V}{W} \quad (1)$$

$$R\% = \frac{C_i - C_f}{Ci} \times 100 \quad (2)$$

where C_i is the initial concentration of As(III) in the solution (mg/L), and C_f is the equilibrium concentration of metal ions in the solution (mg/L), V is the solution volume (L) and W is the mass of adsorbent (g).

3.4. Isotherm study

The maximal adsorption capacity is determined in part by the adsorption isotherm's capacity, which is crucial. Additionally, it provides a brief overview of the steps taken by the system, indicating how effectively an adsorbent will work as an adsorbent, and allowing for an evaluation of the adsorbent's financial viability and potential for use in commercial settings. The use of the Langmuir and Freundlich models (two-parameter models) to describe the biosorption isotherm is fairly widespread in the published literature [72]. Some of the significant

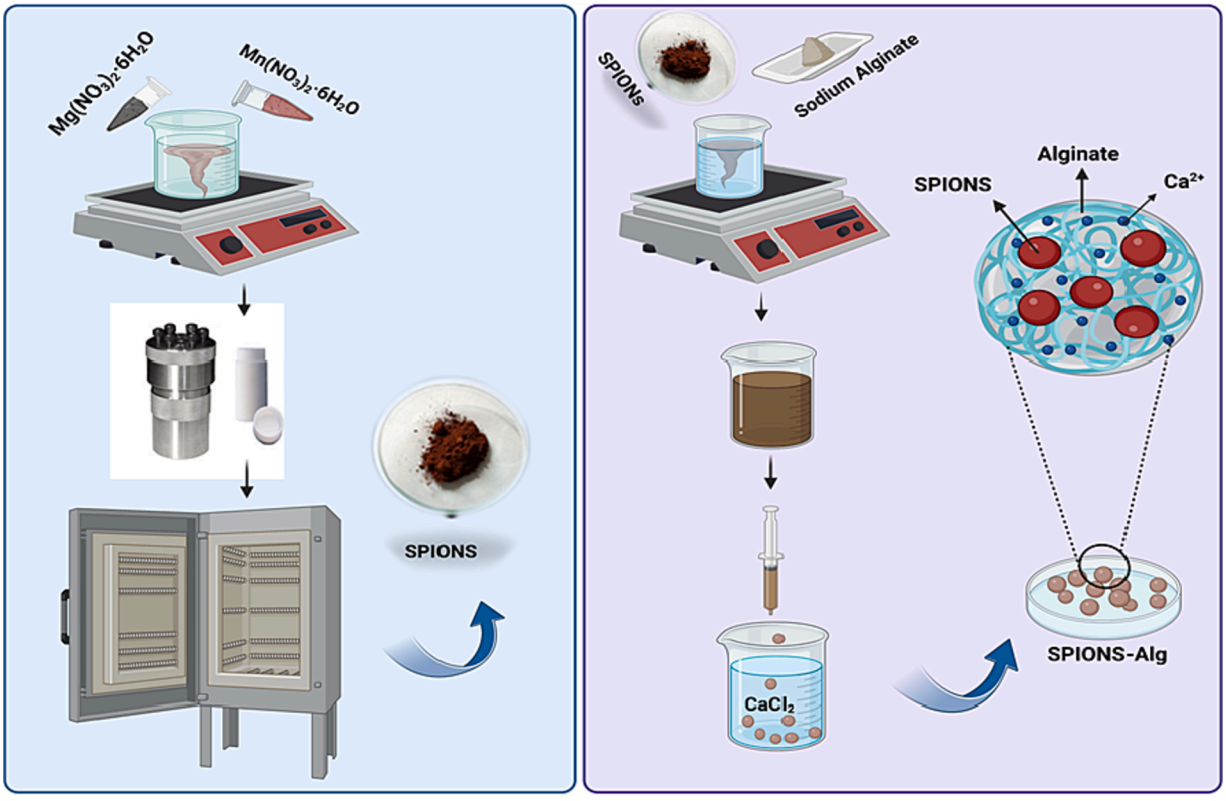

Fig. 1. Schematic diagram for the preparation of SPIONs ($Mg_{1-x}Mn_xFe_2O_4$) by the hydrothermal method and SPIONs-Alg by polymerization of NPs-alginate matrix in $CaCl_2$ solution.

factors usually mentioned for the extensive use of these models include their simplicity, physical meaning, ease of interpretation, and well-established models. Due to their ease of linearization despite their simplicity, two-parameter models are generally favored. Adsorption isotherms (Langmuir and Freundlich) were performed by altering the initial concentration of As(III) in a range of 2.5–7.5 mg/L to explain the equilibrium adsorption features. Then, a plot of qe (As(III) concentration in solid phase at equilibrium) versus C_e (arsenic concentration in solution at equilibrium) was obtained and analyzed. The mathematical and the linear description of the Langmuir equation are represented by equations (3) and (4) [73]:

$$q_e = \frac{q_{max}\, bC_e}{1 + bC_e} \tag{3}$$

$$\frac{1}{q_e} = \frac{1}{K_L q_{max}} \cdot \frac{1}{C_e} + \frac{1}{q_{max}} \tag{4}$$

where, q_e represents the metal concentration on the sorbent (mg/g) at equilibrium, q_{max} is the maximum adsorption capacity (mg/g), C_e is the equilibrium solute concentration in the aqueous solution (mg/L) and K_L is the Langmuir isotherm constant (L/mg) related to the free energy of adsorption between As(III) and adsorbents. To get the separation factor (R_L) equation (5) was used.

$$R_L = \frac{1}{1 + C_i \times K_L} \tag{5}$$

where, R_L is the dimensionless Langmuir constant which indicating whether adsorption is favorable ($0 < R_L$ greater than 1), unfavorable (R_L greater than 1), or irreversible ($R_L = 0$).

The Freundlich model, in contrast to the Langmuir model, implies a distinct heterogeneous adsorption surface and active sites with varying energies [74]. The Mathematical representation and its linear equation can be written as

$$q_e = K_F\, C_e^{(1/n)} \tag{6}$$

$$\text{Log}\, q_e = \text{Log}\, K_F + 1/n \log C_e \tag{7}$$

where k and n are constants for a given adsorbent-adsorbate system.

3.5. Kinetic analysis

Adsorption kinetic models can be used to match experimental data, providing information on the adsorption mechanism, a prospective rate profile, and the viability of chemical adsorption during the adsorption process [75]. In order to illustrate the As(III) biosorption kinetics by SPIONs and SPIONs-Alg, we used pseudo-first order and pseudo-second order models. In equilibrium 8, the pseudo-first order rate expression is shown where k_1 (min^{-1}) is the rate constant of sorption, q_t (mg/g) is the amount of As(III) ions adsorbed at any time t (min) and q_e (mg/g) is the amount of As(III) sorbed at equilibrium. The pseudo-first-order model for As(III) ion adsorption onto sorbents is depicted as linear plots of ln (q_e- q_t) *vs* t.

$$\log(q_e - q_t) = \log q_e - \frac{K_1}{2.303} t \tag{8}$$

In equation (9), pseudo-second order model is represented by equilibrium.

$$\frac{t}{q} = \frac{1}{h} + \frac{1}{q_e} t \tag{9}$$

where q_e (mg/g) is the amount of As(III) sorbed at equilibrium, q_t (mg/g) is the amounts of As(III) sorbed at equilibrium (mg/g) t (min) is time, $h = k_2 * (q_e)^2$ (mg g^{-1} min^{-1}) can be regarded as the initial adsorption rate as $t \rightarrow 0$, and k_2 (g/mg min) is the rate constant of the second-order equation. Finally, linear plots of t/qt *vs* were drawn.

3.6. Adsorption thermodynamics

Thermodynamic studies were performed to identify the thermal effects of sorption and Gibbs free energy (ΔG°) (kJ/mol), which is the essential criterion to establish whether a process happens spontaneously. Standard change in entropy (ΔS°) (J/mol K) and standard change in enthalpy (ΔH°) (kJ/mol) were determined [76]. The values of ΔG°, ΔH° and ΔS° can be obtained from equations (10), 11 and 12, respectively.

$$\Delta G^{\circ} = -RT \ln K^{\circ} \tag{10}$$

$$\ln K^{o} = -\frac{\Delta H^{o}}{RT} + Constant \tag{11}$$

$$\Delta S^{\circ} = \frac{\Delta H^{\circ} - \Delta G^{\circ}}{T} \tag{12}$$

where R is the ideal gas constant (8.3145 $Jmol^{-1}K^{-1}$) and T represents the temperature (K), and K_L (L/mol) is the Langmuir constant. The slope and intercept of the plot of ln K versus 1/T give ΔH and ΔS values, respectively.

3.7. Desorption experiments

Secondary water pollution in water purification systems could be caused by SPIONs leaching from SPIONs-Alg during arsenic adsorption from arsenic-contaminated water. To investigate this potential problem, 0.2 g of SPIONs-Alg was added to 100 mL of deionized water at pH 7 and 30 °C for 120 min while shaking at 150 rpm. SPIONs-Alg beads were separated with a magnet, and the supernatant was looked at to see if any SPIONs had leached into the aqueous solution. The suitability of synthesized SPIONs and SPIONs-Alg was assessed using consecutive adsorption–desorption cycles. The adsorption process was carried out under optimum conditions, and the supernatant was analyzed for metal ion concentration. The adsorbents were then collected from the solution, washed with distilled water, and dried. Then, to estimate the desorption ability, dried adsorbents were contacted with 100 mL of HCl and NaOH at the following concentrations (0.01, 0.1, and 1.0 M) in 250 mL Erlenmeyer flasks to allow metal ions to be released from the adsorbents [77].

The regeneration efficiency was measured by the following equation:

$$\text{Desorption efficiency}\,\% = \frac{\text{Amount of metal desorpted(mg)}}{\text{Amount of metal loaded(mg)}} \times 100 \tag{13}$$

In order to detect high desorption at low values of the solid-to-liquid (S/L) ratio, various S/L ratios (0.5, 1, 1.5, and 2) were tested. The S/L ratio is defined as the ratio of metal-laden adsorbent to the volume of the elutant. The desorption process was carried out after determining the optimum eluent concentration and solid-to-liquid ratio. To assess the adsorbents' potential for reuse, the regenerated samples were collected following each procedure, washed, dried, and used again for As(III) removal for up to eight consecutive regeneration cycles [69].

4. Results and discussion

4.1. Materials characterization

In the current study, two adsorbents, SPIONs and SPIONs-Alg, were successfully synthesized. The FESEM micrograph displayed nearly spherical-shaped SPIONs with grain sizes below 30 nm (Fig. 2). Despite the fact that these smaller crystallites are uniformly dispersed across the whole region and exhibit fine grain development, a distinct border between nearby crystallites can be recognized, with occasional agglomeration caused by the interactions of magnetic nanoparticles. The disparity between XRD-calculated particle size and FESEM-observed particle size may be related to molecular structural disorder and

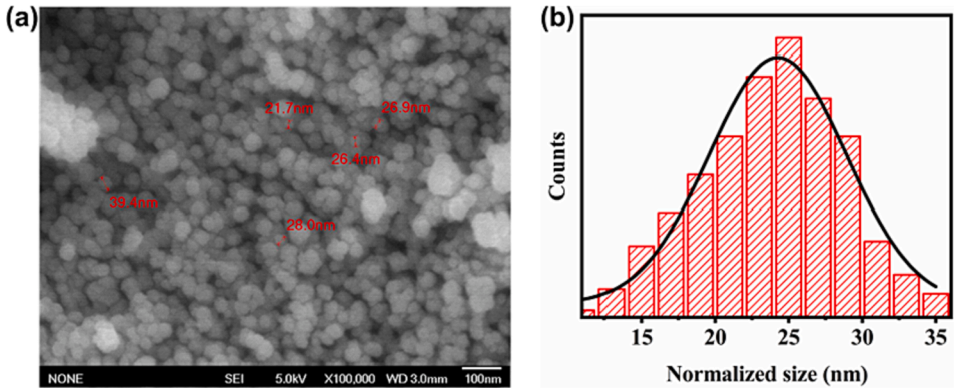

Fig. 2. (a) FESEM image, and (b) particle size distribution histograms of SPIONs.

lattice strain, which are caused by the nanoparticles' differing ionic radii and/or clustering. The aggregation is indicative of the sample's high reactivity following heat treatment, which may result from magnetostatic or exchange interactions between particles. When nanoparticles encounter a persistent magnetic moment proportionate to their volume, they tend to agglomerate [78].

Fig. 3a represents the indexed XRD patterns of the synthesized samples (SPIONs and SPIONs-Alg) using the hydrothermal method. The formation of single-phase cubic spinel structures for both samples was validated, and no additional phase was detected. The hkl indices of the samples were (220), (311), (400), (511), and (440). These planes reveal the presence of a mixed type cubic spinel structure. The crystallite sizes (25 nm) were calculated using the Debye-Scherrer equation, $D = \frac{k\lambda}{\beta\cos\theta}$, where, D is crystallite size, λ is the wavelength of radiation and β is full width at half maxima (FWHM) centered at 2θ of intense peak (311). The similar diffraction patterns of SPIONs and Alg indicate that alginate coating had no effect on the crystalline structure of SPIONs [79]. This indicates that the alginate coating occurs only at the surface of SPIONs [80]. The decrease in the sharpening of the peaks of SPIONs-Alg is due to the increase in size after alginate coating.

To elucidate the functional groups in the surface of the sorbents, FTIR analysis was carried out with the data shown in Fig. 3b. Samples a and b represent SPIONs and SPIONs-Alg, respectively. The two main broad metal–oxygen bands are seen in the IR spectra of all spinel ferrites [81]. The band that appeared at approximately 3400 cm^{-1} is related to the symmetric vibration of O—H groups in the absorbed water of these samples. Besides, the bands noted at 2936 cm^{-1} refers to the stretching vibration of the aliphatic C—H. The band around 600 cm^{-1} could be attributed to the intrinsic stretching vibrations of the metal–oxygen [Fe–O] bond, and the bands at 400 cm^{-1} correspond to vibration of octahedral [Fe–O] bond [82]. This band is clearly evidence of the ferrite formation in spinel form, which is matched with the XRD pattern of SPIONs. The absorption peak around 400 cm^{-1} is not clearly visible in FTIR due to the limited device measuring range. Nevertheless, in the case of SPIONs-Alg, the band at 585 cm^{-1} appeared with a high intensity, confirming the existence of the nanoferrite. The infrared spectra of SPIONs-Alg demonstrate that the peaks around 1600 and 1400 cm^{-1} represent the asymmetric and symmetric stretching vibrations of the carboxylate groups, respectively [83]. Moreover, SPIONs-Alg has an ether C—O stretching vibration peak at about 1030 cm^{-1}.

The specific surface area was determined using the BET technique. The volumetric measurement method was used, which provides accurate readings. Fig. 4a illustrates the BET results of SPIONs and SPIONs-Alg. The specific surface areas of SPIONs and SPIONs-Alg were 30.27 and 37.21 m^2/g, respectively. The addition of alginate to SPIONs improves the specific surface area, ensuring adequate stability [84]. Fig. 4b demonstrates the zeta potential of SPIONs and SPIONs-Alg. The zeta potentials of SPIONs and SPIONs-Alg were found to be −36 mV and −48 mV, respectively [85]. The results showed that following stabilization with alginate polymer, the SPIONs stability was enhanced, which is in good agreement with the result of BET measurements.

Fig. 5 depicts the hysteresis loops of both SPIONs and SPIONs-Alg at room temperature. These hysteresis loops are used to determine magnetic parameters such as saturation magnetization (M_s), remanence (M_r), and coercivity (H_c). The leading magnetic phase for both samples at room temperature is determined to be superparamagnetic due to the

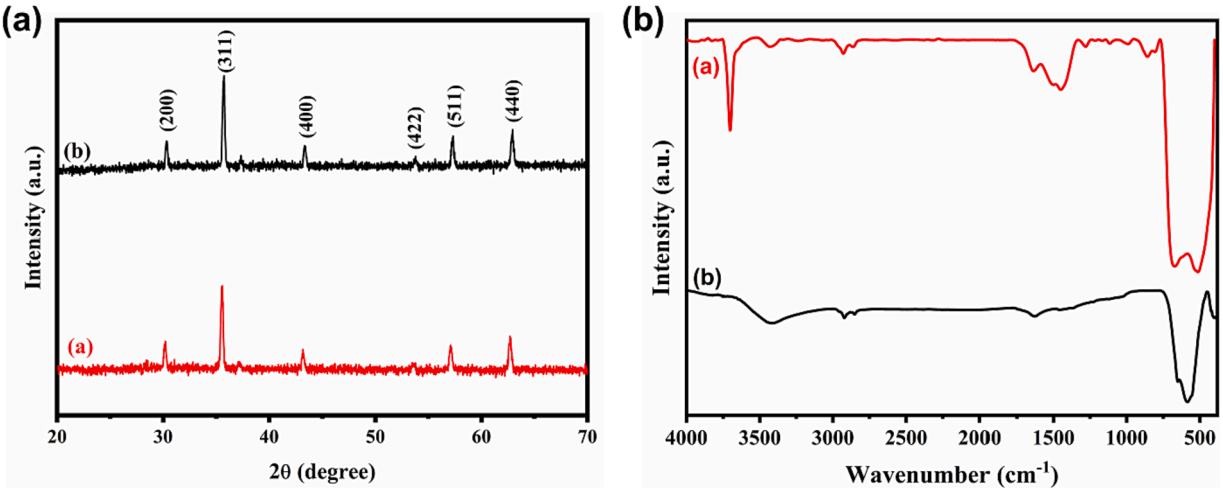

Fig. 3. A) Xrd spectra for (a) SPIONs-Alg and (b) SPIONs. b) FTIR spectra of synthesized adsorbents; (a) SPIONs-Alg and (b) SPIONs.

(a)

Sample	Specific surface area $m^2 g^{-1}$
SPIONs	30.27
SPIONs-Alg	37.21

(b)

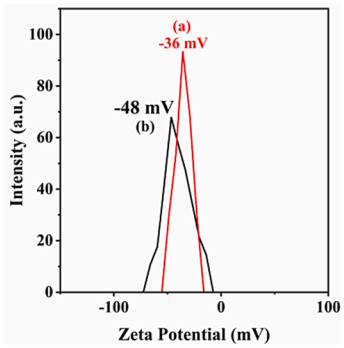

Fig. 4. (a) BET (specific surface area measurements) and (b) Zeta potentials of (a) SPIONs (b) SPIONs-Alg.

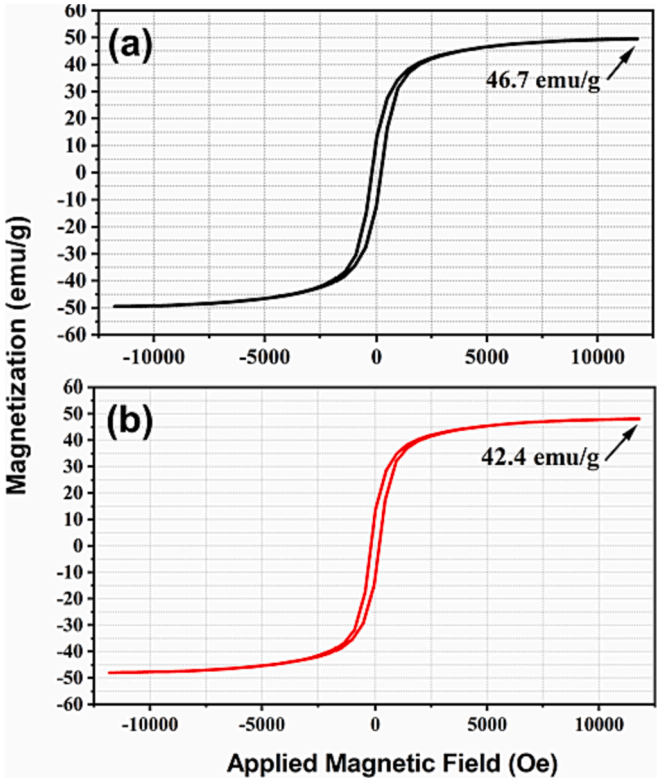

Fig. 5. Magnetization versus applied magnetic field for (a) SPIONs and b) SPIONs-Alg.

S-like form of the loops, which do not have coercivity [86]. Although SPIONs ($Mg_{0.5}Mn_{0.5}Fe_2O_4$) is soft cubic ferrites, one can expect some magnitude of coercivity, as reported elsewhere [87]. However, the samples' observed superparamagnetic activity suggested that the size range of synthesized particles (25–30 nm) is smaller than the required size to see ferrimagnetic behavior. This was determined by comparing the size range to the crucial size [88]. After coating, there is a marked decrease in the saturation magnetization of SPIONs. It is suggested that the mass ratio of magnetic material decreases after coating in each capped particle, which in turn results in a decrease in the saturation magnetization. This is because saturation magnetization is proportional to the mass ratio of the magnetic material that is contained inside the organic layer [89]. The inversion degree brought on by surface spin-canting and the finite size effect bring to a reduction in magnetization in spinel ferrite nanostructured materials, bringing the value down from 46 emu/g to 42 emu/g.

4.2. Effect of contact time on As(III) adsorption

Another crucial operational characteristic for a cost-effective wastewater treatment process is the equilibrium time. To explore the effect of contact time on the arsenic elimination by the synthesized (SPIONs and SPIONs-Alg) sorbents, removal times between 0 and 180 min were selected, and the related outcomes are shown in Fig. 6a. From the results, a two-stage behavior was observed. Indeed, the percentage of As(III) uptake increased with time, reaching maximum values (43% and 51%) at 40 and 120 min for SPIONs and SPIONs-Alg, respectively. Consequently, it is likely that during the first phase of the process, all sites on the surfaces of the adsorbents were readily available, and the concentration gradient of the adsorbate was extremely large, resulting in a greater absorption rate [90]. As a result, as removal time increased, the percentage of arsenic uptake remained constant. This result could be explained by the fact that, at times over the optimum removal time, a saturation phase was formed, so As (III) desorption and adsorption repeated again and the removal percentage stayed constant [91].

4.3. Effect of adsorbent dosage on As(III) adsorption

Since maximizing the interactions between metal ions and adsorption sites of adsorbent in the solution fundamentally requires an optimal adsorbent dose, the impact of sorbent concentration on the elimination percentage of arsenate was examined using 0–3 g/L of sorbent. From Fig. 6b, arsenic removal efficiency increased to 88% and 99% for SPIONs and SPIONs-Alg, respectively, when the sorbent concentration was raised from 0.5 to 2.5 and 2 g/L. This result can be explained by the claims that more surface area was made available during the adsorption process with the increase in the adsorbent dose. Therefore, raising active sites leads to a growing arsenic removal percentage [92]. However, as concentrations rose above 2.5 and 2 g/L for SPIONs and SPIONs-Alg, respectively, removal efficiency did not change. This happens as a result of the solution ion concentration decreasing at increasing adsorbent doses, the system reaches equilibrium while the adsorption sites remain unsaturated [93]. So, for further experiments, 2.5 g/L of SPIONs and 2 g/L of SPIONs-Alg were chosen as the optimum sorbent dose.

4.4. Effect of temperature and initial concentration on As(III) adsorption

The effect of temperature on the arsenic removal efficiency of the synthesized adsorbents was examined in batch adsorption experiments at different temperatures (10 °C, 20 °C, 30 °C, 40 °C, 50 °C, and 60 °C). Because of the endothermic nature of the adsorption process onto the synthesized adsorbents, As(III) adsorption increased from 10 °C to 30 °C. Furthermore, because temperature influences the interaction between metal ions and sorbent, increasing the temperature increases the diffusion rate of As(III) ions (Fig. 6c); this result is consistent with previous research [94]. However, after 30 °C, the removal of As(III) ions by adsorbents decreased with increasing temperature. A higher temperature

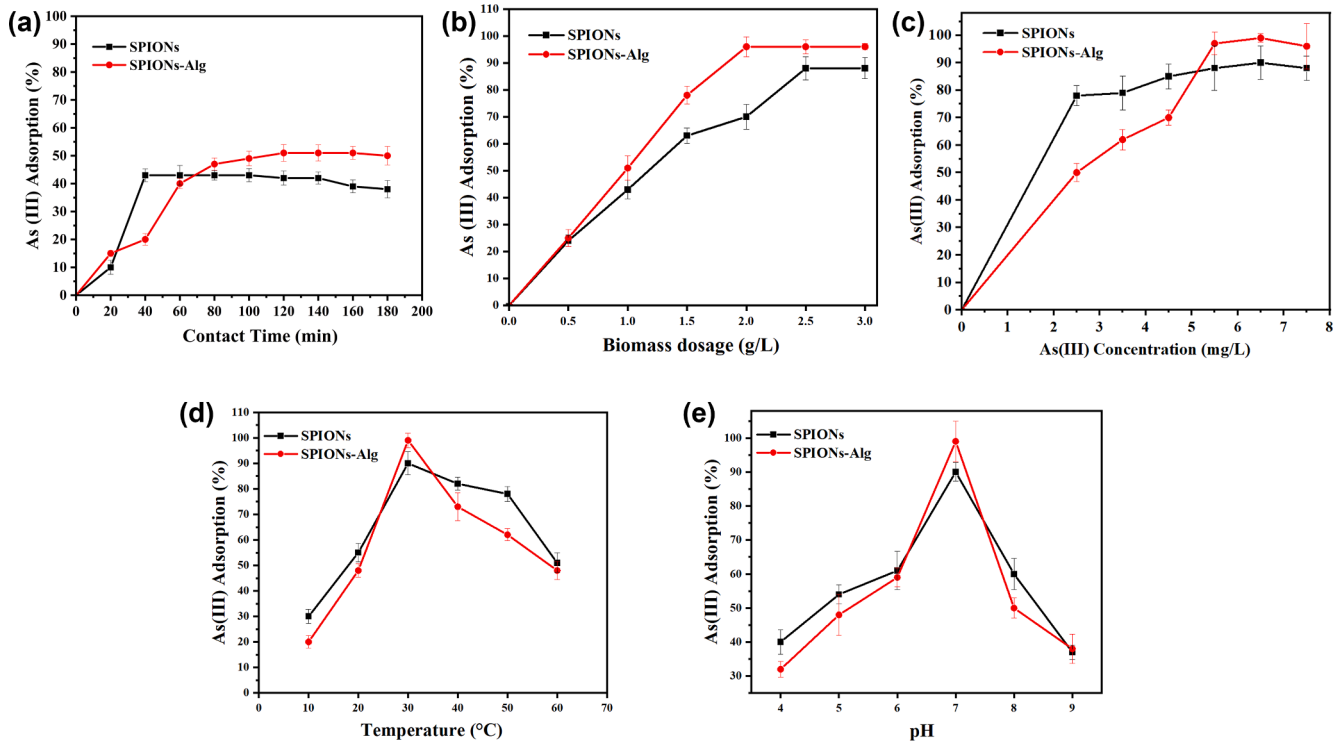

Fig. 6. Effects of **a**; contact time (0–180 min) **b**; adsorbent dosage (0.5–3 g/l) **c**; As(III) concentration (0–7.5 mg/L) **d**; temperature (10–50 °C) and **e**; PH (2–9) on adsorption of As(III) ions at 150 rpm.

resulted in a lower efficiency for As(III) removal due to a variety of factors, including the destruction of some active sites on the adsorbent's surface or deactivation of the sorbent due to bond breaks and weakening of the adsorptive forces between the As(III) ions and the active sites of the adsorbent [95]. So, for further experiments, 30 °C was chosen as the optimum temperature [96].

Furthermore, the effect of the initial As(III) concentration on the removal of As(III) by adsorbents was investigated in the 0–7.5 mg/L range, and the results are shown in Fig. 6d. The percentage of arsenic adsorption increased with increasing initial As(III) concentration and reached a saturation value of 6.5 mg/L for both sorbents. Higher interactions between the As(III) and adsorbent molecules may be the cause of the increased adsorption capabilities [97]. However, as the concentration of As(III) increased, the removal percentage decreased due to a decrease in accessible active sites at higher concentrations [98].

4.5. Effect of pH on As(III) adsorption

In the metal adsorption process, pH is an imperative factor, as it has a crucial impact on metal ion speciation in the solution and functional groups existing on the adsorbent surface [99]. As a result, the binding capacity of adsorbents for adsorbing As(III) ions varied with pH. The effect of pH on the removal of As(III) by synthesized SPIONs and SPIONs-Alg is depicted in Fig. 6e. Separately, the optimal amount of adsorbents was added to 100 mL of As(III) solution (6.5 mg/L) at different pH (4–9) levels and then placed in a shaking incubator for 40 and 120 min. The removal of As(III) increased rapidly as the pH of the solution increased from 4 to 6, with the maximum As(III) adsorption by all adsorbents occurring at pH 7. The plots show that the efficiency of As (III) adsorption increased to a maximum at pH 7, where SPIONs and SPION-Alg adsorbed 90% and 99%, respectively. This result indicated that the arsenic adsorption efficiency of these sorbents was pH-dependent.

Adsorption can occur through ion-exchange of surface carboxyl groups and As(III) ions in the solution. The findings revealed that in acidic media, carboxyl groups have more protons (H^+) available to them. As a result, As(III) ions compete with hydrogen ions for protonated active sites. Therefore, a high level of protons can reduce the available binding sites on an adsorbent's surface [100]. It is a plausible explanation for the low As(III) uptake in acidic environments. Furthermore, as the pH increased, the number of negatively charged positions available for As(III) ion binding increased. Arsenic adsorption in alkaline solution increases as the amount of OH^- increases [101]. Arsenic adsorption does not merely depend on the availability of active sides on the adsorbent surface; it also depends on the arsenic chemical changes in the aqueous medium. It was previously found by numerous researchers that arsenic occurs in non-ionized (neutral) form as H_3AsO_3 and in ionized forms such as H_2AsO_3, $HAsO_3^{2-}$ and H_2AsO^{3-} at a pH range of 3–11 [102]. Adsorption capability decreased significantly at pH greater than 7 due to changes in adsorbent properties and As(III) ionic forms [103]. Because SPIONs-Alg achieved the highest As(III) adsorption, this can be explained by the fact that the presence of ferrite NPs implanted in alginate beads increases the number of active [70,96,104].

4.6. Adsorption isotherm

The capacity of the sorbents (SPIONs and SPIONs-Alg) to remove As (III) from the solution was shown using Langmuir and Freundlich isotherm models in Fig. 7. These models also demonstrated a link between the surface characteristics and affinity of the sorbent in the batch culture and the efficacy of arsenic removal. The Langmuir isotherm explains the monolayer adsorption of pollutants onto the adsorbent surface with a finite number of adsorption sites, whereas the Freundlich isotherm supports the idea that adsorption happens on the adsorbent's heterogeneous surface [105]. According to the results presented in Table 1, Langmuir's isotherm was the best fit because the values of the coefficients of determination (R^2) were found to be 0.9729 for SPIONs and 0.9955 for SPIONs-Alg. As(III) ion sorption onto adsorbents was thus defined as monolayer adsorption because it occurred at functional groups or binding sites on the surfaces of the sorbents [106]. On the

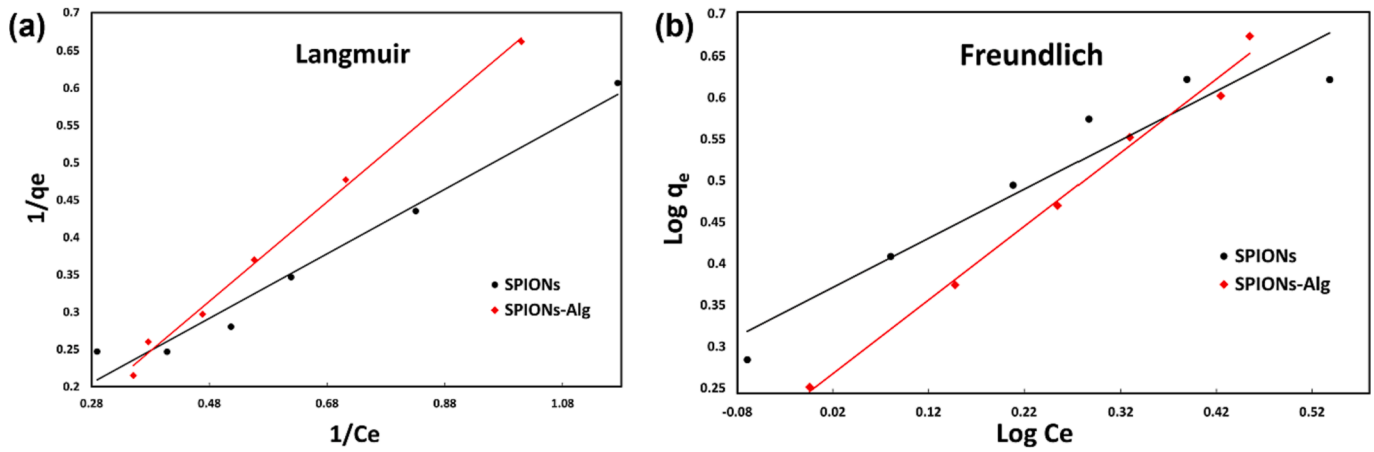

Fig. 7. As(III) adsorption isotherm models (**a**; Langmuir and **b**; Freundlich) by SPIONs and SPIONs-Alg at pH 7, 30 °C.

Table 1
Isotherm models' parameters for biosorption of As(III) onto SPIONs and SPIONs-Alg.

Adsorbent	Langmuir			Freundlich		
	b	q_{max} mg/g	R^2	K_F (mL/mg)	n	R^2
SPIONs	0.1945	11.89	0.9729	1.503	0.974	0.98
SPIONs-Alg	0.0073	204.081	0.9955	2.0137	1.462	0.91

other hand, R^2 values for the Freundlich isotherm model were found to be just 0.916 for SPIONs and 0.9899 for SPIONs-Alg. According to these findings, the Freundlich model was unable to adequately define the relationship between the percentages of As(III) adsorbed and their equilibrium concentrations in solution. The maximum adsorption capacity (qmax) of SPIONs-Alg for As(III) was found to be 204.081 mg/g, which is significantly higher than the value of SPIONs, which is 11.89 mg/g. Table 2 compares the arsenic adsorption capabilities of the sorbents used in the present study with those of other different sorbents reported in the literature. Because the separation factor (RL) values for both sorbents are less than one, the adsorption phenomena are favorable.

4.7. Determination of kinetics rate

The measurement of biosorption rates, which are crucial for figuring out the ideal operating parameters for full-scale batch processes, can provide important information for constructing biosorption systems. The kinetics of As(III) adsorption onto SPIONs and SPIONs-Alg were represented using pseudo-first-order and pseudo-second-order models. Fig. 8 depicts the fitting of two kinetic models to the As(III) equilibrium data, and Table 3 shows the results of the corresponding kinetic parameters. The pseudo-first-order model was unsuitable for simulating As (III) adsorption onto both sorbents because the values of R^2 are low and the values of q_e, exp are not in good agreement with the theoretical values obtained (q_e) from equilibrium 5. In comparison to pseudo-first order kinetics, pseudo-second order kinetics was found to be the best fit model for explaining the kinetics of As(III) adsorption on both sorbents, as evidenced by a higher linear regression coefficient (R^2 0.9904 for SPIONs and R^2 0.9965 for SPIONs-Alg). Furthermore, there is a logical agreement between the experimental and theoretical adsorption capacity (q_e) values, favoring the pseudo-second-order kinetic model. The greatest fit for the data is provided by a model that presupposes that the rate-limiting phase may be controlled by chemical sorption involving valence forces through the exchanging or sharing of electrons among sorbent and sorbate [116]. These findings support previous research and demonstrate a strong correlation between the second-order equation and adsorption experiments [117–119].

Table 2
Comparison of the As(III) adsorption capacity of synthesized adsorbents with those previously reported.

Adsorbent	Adsorption capacity (mg/g)	PH	Reference
Chitosan-magnetic-graphene oxide (CMGO)	45	7.3	[107]
γ-Fe2O3-TiO2-GO	110.4	6.5	[108]
Goethite calcium alginate (Cal-Alg-Goe)	30.44	6	[109]
Magnetic nanoparticles coated zeolite (MNCZ)	19.39	2.5	[110]
MFMNABs	6.6533	7	[111]
Graphene Oxide–$MnFe_2O_4$ Magnetic Nanohybrid	97	6.5	[112]
Fe–Mn binary oxide	132.6	7.7	[113]
Carbon nanotubes (MWNT/f)	109.457	7	[114]
Bacteria/Sawdust/$MnFe_2O_4$ composite	87.573	7	[115]
$CoFe_2O_4$	100	7	[63]
$MnFe_2O_4$	94	7	[63]
SPIONs	11.89	7	This study
SPIONs-Alg	240.081	7	This study

4.8. Adsorption thermodynamics

Adsorption thermodynamics is used to determine if the adsorption process is spontaneous or not. The nature of the adsorbent and adsorbate is also predicted at equilibrium. Additionally, it makes predictions about the ideal conditions for the feasibility of the adsorption process and looks into the range of temperatures at which the adsorption process is favorable or unfavorable. Along with the spontaneity of the adsorption process, the endothermic or exothermic nature of the sorption reaction can be determined using the thermodynamic parameters of enthalpy (ΔH°), entropy (ΔS°) and Gibbs free energy (ΔG°) of the sorption. Fig. 9 shows the graph of ln k^o against 1/T, and Table 4. lists the relevant data obtained from the equations (10–12). As(III) adsorption increased with increasing temperature, and was found to be positive. The presence of a strong interaction between sorbents and As(III) was confirmed by the positive value of ΔH° indicating that the adsorption process for As(III) is endothermic. Endothermic reactions happen when the enthalpy of the products is higher than the enthalpy of the reactants. This means that heat energy is taken in from the environment [57].

The standard free energy change (ΔG°) can be used to predict whether or not the adsorption process is thermodynamically feasible; if the ΔG° < 0, the adsorption process is always feasible and spontaneous, whereas if the ΔG° greater than 0, the adsorption process is non-feasible and non-spontaneous [120]. The results showed that the adsorption

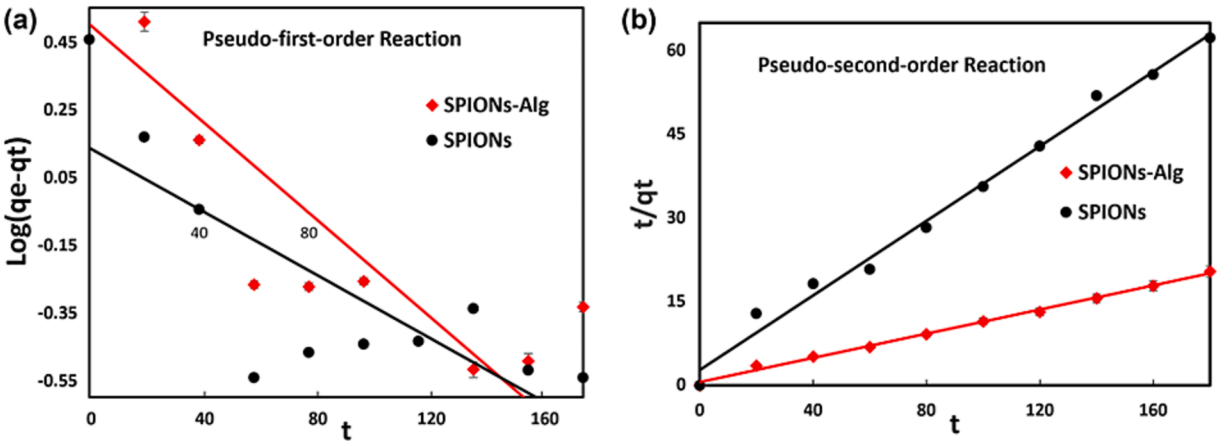

Fig. 8. Kinetic models for As(III) sorption. (a) and (b) Pseudo-first and second order models for SPIONs and SPIONs-Alg.

Table 3
Kinetic parameters for biosorption of As(III) onto SPIONs and SPIONs-Alg.

Adsorbent	Pseudo-first order Reaction			Pseudo-second order Reaction		
	R^2	q_e	K_1	R^2	q_e	K_2
SPIONs	0.62	1.535	0.0019	0.9904	2.99	24.78
SPIONs-Alg	0.69	3.556	0.003	0.9965	9.22	49.298

reaction was feasible and spontaneous because the Gibbs free energy change (ΔG°) was negative at various temperatures. The decrease in ΔG° values as temperature increased indicated that at higher temperatures, efficient adsorption was greater. Because ions are easily dehydrated at higher temperatures, their adsorptions become more favorable [121]. Positive entropy change (ΔS°) values may indicate structural changes in the sorbents as well as the adsorbents' affinity for As(III) ions in aqueous solutions. During arsenic adsorption onto SPIONs and SPIONs-Alg, the results showed a higher randomness tendency at the adsorbents and adsorbed materials interface. The equilibrium uptake of arsenic ions was found to be temperature-dependent, increasing with temperature rises up to 30 °C (313.15 K). When the temperature was raised to 40 °C (313.15 K), the process became unstable. The data for temperatures higher than 30 °C (303.15 K) were left out in Fig. 9 since they would have affected the trend that was being illustrated, so it can be noted that 10 °C to 30 °C was the suitable condition for the adsorption process. These recent findings are similar to those in earlier research [122].

4.9. Desorption and regeneration

During arsenic adsorption, SPIONs were leached from SPIONs-Alg. The total SPIONs concentration leached from the SPIONs-Alg was 0.014 mg/L. Since SPIONs and alginate establish powerful chemical interactions, some SPIONs in SPIONs-Alg could not bind tightly to the alginate and leached out into the water. This can be because there are fewer binding sites on the polymer matrix and all functional groups have been consumed. SPIONs were leached at a very low concentration (0.014 mg/L), confirming the strong impregnation of SPIONs into the beads and reducing the risk of secondary contamination. The leaching investigation also confirms that the adsorbent is stable and that it can be applied to the treatment of water as well as other possible environmental applications [93].

As a practical matter, reusability is an essential aspect of an advanced adsorbent [53]. Adsorbents with higher adsorption capacity and better

Table 4
Thermodynamic parameters for adsorption of As(III) onto SPIONs and SPIONs-Alg.

Adsorbent	Temperature K	ΔG° (kJ/mol)	ΔH° (kJ/mol)	ΔS° (J/mol K)
SPIONs	283.15	−0.08	61.148	0.216
	293.15	−2.242		
	303.15	−4.405		
SPIONs-Alg	283.15	−0.029	22.933	0.081
	293.15	−0.839		
	303.15	−1.650		

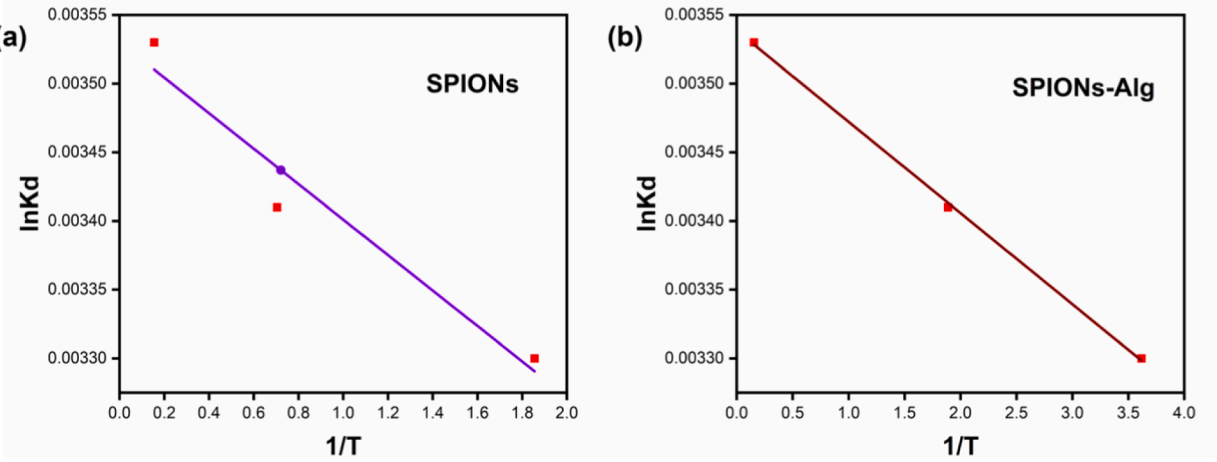

Fig. 9. Adsorption thermodynamics at different temperatures (283.15, 293.15 and 303.15 K) for As(III) for SPIONs and SPIONs-Alg.

desorption characteristics can reduce the overall cost of the adsorption process. To evaluate practical applications and economics, the regeneration possibilities of SPIONs and SPIONs-Alg were studied. The choice of eluents is significantly influenced by the type of sorbent and the adsorption mechanism. Additionally, the eluent should possess certain essential qualities, including: not harming the adsorbent, affordability, environmental friendliness, and effectiveness. Researchers have previously looked at a variety of chemical agents to desorb metals from various adsorbents, and most of them concluded that mineral acids and alkaline eluent agents may achieve a higher percentage of desorption efficiency [123]. The recovery of adsorbed As(III) ions was examined by using different concentrations (0.01, 0.1, and 1.0 M) of eluents such as HCl and NaOH. The best elution was achieved using 0.1 M NaOH solution, and the As(III) ion recovery percentage in SPIONs-Alg and SPIONs was determined to be 91% and 82%, respectively (Fig. 10a), which are in line with previous studies that reported alkaline solution as a desirable regenerating agent for anion recovery from polymer-based composite adsorbents. This efficiency was caused by the impregnated metal oxides' strong affinity for hydroxyl ions [124]. Most of the surface sites of SPIONs-Alg are negatively charged at high alkaline pH, and competition between complexed ligands and hydroxyl ions induces ligand desorption [70].

In order to determine the ideal solid-to-liquid (S/L) ratio in the presence of 0.1 M NaOH, tests were conducted. High As(III) recovery can be obtained at S/L ratios of 1.5 g/l for SPIONs-Alg and 2 g/l for SPIONs (Fig. 10b). Elution efficiency decreased at S/L ratios greater than 1.5 g/l and 2 g/l for metal recovery. Due to the thick suspension that was made, there was not much interaction between the adsorbent and the NaOH. This may be why the elution efficiency values at high S/L ratios [119,120] were not very good [125,126].

Through the eight following adsorption–desorption cycles, the reusability of the sorbents was tested. Fig. 10c demonstrates that SPIONs-Alg can be used frequently in As(III) with no significant loss in total adsorption capacity after five cycles. While the As(III) removal percentage of SPIONs was found to be greater than 90% during the first three adsorption–desorption cycles, it gradually decreased on subsequent cycles. SPIONs immobilized in alginate beads are mechanically and chemically stronger and more favorable to regeneration for multiple cycles than non-immobilized ones. The inability of the granulated or non-immobilized SPIONs to regenerate may be attributed to their disintegration with the corrosive effects of an alkaline solution as well as their wettability and dispersibility in water. The early deactivation of the particles, weak mechanical strength, and separation of used particles from any flow-through system can all be resolved by immobilizing SPIONs inside alginate beads [127].

5. Conclusion

Novel superparamagnetic iron oxide nanoparticles $Mg_{0.5}Mn_{0.5}Fe_2O_4$ (SPIONs) and superparamagnetic iron oxide nanoparticles alginate beads (SPIONs-Alg) were successfully synthesized. By characterization, the size of SPIONs was determined to be 25 nm, and the specific surface area of SPIONs and SPIONs-Alg was 30.27 and 37.21 $m^2\ g^{-1}$, respectively. In addition, the zeta potentials of SPIONs (-36 mV) and SPIONs-Alg (-48 mV) were determined. The arsenic removal efficiency of the adsorbents (SPIONs 90% and SPIONs-Alg 99%) was optimized in bath culture. SPIONs and SPIONs-Alg obtained maximal adsorption in 40 and 120 min at neutral pH 7 and 30 °C, respectively. The sorption characteristics of both sorbents supported the idea that the adsorption process could be better described by the pseudo-second-order kinetic (chemisorption through electron exchange) and Langmuir models. The Langmuir sorption capacity was determined to be 11.89 mg/g for SPIONs and 204.081 mg/g for SPIONs-Alg (monolayer sorption). The thermodynamic characteristics demonstrated that the adsorption of As(III) was endothermic, practicable, and spontaneous. Arsenic could be easily desorbed from adsorbents using a 0.1 M NaOH solution, and the adsorbents could be isolated from the solution using a magnet and reused as sorbents (SPIONs) for three and (SPIONs-Alg) five regeneration cycles. Consequently, we reported herein for the first time that SPIONs-Alg can be used as a promising adsorbent for selective separation and recovery of As(III) from aqueous solutions due to its high efficiency, fast kinetics, and good reusability, as well as its low cost, simple preparation, and convenient separation. The upgrading of these composite materials for use in large-scale wastewater treatment facilities requires more study. Future research may also concentrate on the post-treatment of the by-products of such a complicated sorbate-sorbent system.

Data and code availability

The authors confirm the absence of sharing data.

CRediT authorship contribution statement

Somayeh Asadi Haris: Conceptualization, Data curation, Formal analysis, Methodology, Visualization, Writing – original draft, Writing – review & editing. **Shadab Dabagh:** Data curation, Formal analysis, Methodology, Visualization, Writing – original draft, Writing – review & editing. **Hamidreza Mollasalehi:** Data curation, Formal analysis, Writing – original draft. **Yavuz Nuri Ertas:** Conceptualization, Funding acquisition, Project administration, Resources, Supervision, Visualization, Writing – original draft, Writing – review & editing.

Declaration of Competing Interest

The authors declare that they have no known competing financial interests or personal relationships that could have appeared to influence

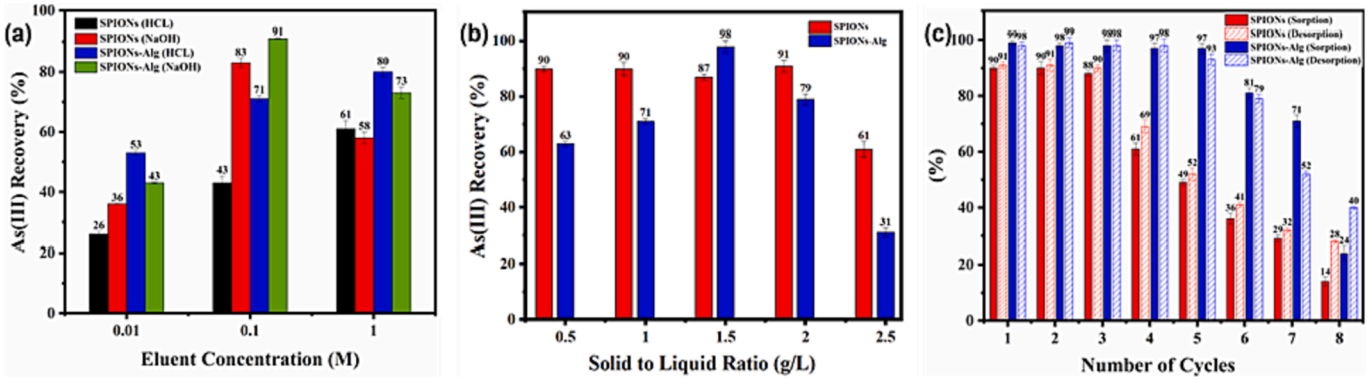

Fig. 10. (a) Regeneration of adsorbed As(III) ions by using different concentrations (0.01, 0.1, and 1.0 M) of eluents such as HCl and NaOH. (b) Solid-to-liquid (S/L) ratio in the presence of 0.1 M NaOH. (c) Reusability of the sorbents through eight following adsorption–desorption cycles.

the work reported in this paper.

Data availability

Data will be made available on request.

Acknowledgements

This research was supported by 2232 International Fellowship for Outstanding Researchers Program of TÜBİTAK (Project No: 118C346).

References

[1] S. Lata, S. Samadder, Removal of arsenic from water using nano adsorbents and challenges: a review, J. Environ. Manage. 166 (2016) 387–406.
[2] J. Yang, et al., Nanomaterials for the removal of heavy metals from wastewater, Nanomaterials 9 (3) (2019) 424.
[3] H.H. Savenije, Why water is not an ordinary economic good, or why the girl is special, Physics and Chemistry of the Earth, Parts A/B/C 27 (11–22) (2002) 741–744.
[4] A. Bhatnagar, M. Sillanpää, Utilization of agro-industrial and municipal waste materials as potential adsorbents for water treatment—a review, Chem. Eng. J. 157 (2–3) (2010) 277–296.
[5] M. Jang, et al., Mechanisms of arsenate adsorption by highly-ordered nano-structured silicate media impregnated with metal oxides, Environ. Sci. Tech. 37 (21) (2003) 5062–5070.
[6] U. Epa, United States environmental protection agency, Quality Assurance Guidance Document-Model Quality Assurance Project Plan for the PM Ambient Air 2 (2001) 12.
[7] W.H. Organization, Organotins in drinking-water, World Health Organization, 2020.
[8] T.G. Asere, C.V. Stevens, G. Du Laing, Use of (modified) natural adsorbents for arsenic remediation: a review, Sci. Total Environ. 676 (2019) 706–720.
[9] A. Basu, et al., A review on sources, toxicity and remediation technologies for removing arsenic from drinking water, Res. Chem. Intermed. 40 (2) (2014) 447–485.
[10] K.S.M. Abdul, et al., Arsenic and human health effects: A review, Environ. Toxicol. Pharmacol. 40 (3) (2015) 828–846.
[11] J.S. Uppal, Q. Zheng, X.C. Le, Arsenic in drinking water—recent examples and updates from Southeast Asia, Current Opinion in Environmental Science & Health 7 (2019) 126–135.
[12] V.M. Nurchi, et al., Arsenic toxicity: molecular targets and therapeutic agents, Biomolecules 10 (2) (2020) 235.
[13] M. Ashrafizadeh, et al., (Nano)platforms in bladder cancer therapy: Challenges and opportunities, Bioeng. Transl. Med. (2022).
[14] P. Sudilovskiy, et al., Use of membranes for heavy metal cationic wastewater treatment: flotation and membrane filtration, Clean Techn. Environ. Policy 9 (3) (2007) 189–198.
[15] H.A. Qdais, H. Moussa, Removal of heavy metals from wastewater by membrane processes: a comparative study, Desalination 164 (2) (2004) 105–110.
[16] M.J. Gonzalez-Munoz, et al., Recovery of heavy metals from metal industry waste waters by chemical precipitation and nanofiltration, Desalination 200 (1–3) (2006) 742–744.
[17] A. Dominguez-Ramos, et al., Arsenic removal from natural waters by adsorption or ion exchange: an environmental sustainability assessment, Ind. Eng. Chem. Res. 53 (49) (2014) 18920–18927.
[18] A. Abejón, A. Garea, A. Irabien, Arsenic removal from drinking water by reverse osmosis: Minimization of costs and energy consumption, Sep. Purif. Technol. 144 (2015) 46–53.
[19] V. Pallier, et al., Effect of organic matter on arsenic removal during coagulation/flocculation treatment, J. Colloid Interface Sci. 342 (1) (2010) 26–32.
[20] D. Syam Babu, P. Nidheesh, A review on electrochemical treatment of arsenic from aqueous medium, Chem. Eng. Commun. 208 (3) (2021) 389–410.
[21] L. Hao, et al., A critical review on arsenic removal from water using iron-based adsorbents, RSC Adv. 8 (69) (2018) 39545–39560.
[22] S. Alka, et al., Arsenic removal technologies and future trends: a mini review, J. Clean. Prod. 278 (2021), 123805.
[23] P. Zito, H.J. Shipley, Inorganic nano-adsorbents for the removal of heavy metals and arsenic: a review, RSC Adv. 5 (38) (2015) 29885–29907.
[24] B. Ekka, et al., Removal of Cr (VI) by silica-titania core-shell nanocomposites: In vivo toxicity assessment of the adsorbent by Drosophila melanogaster, Ceram. Int. 47 (13) (2021) 19079–19089.
[25] B. An, D. Zhao, Immobilization of As (III) in soil and groundwater using a new class of polysaccharide stabilized Fe–Mn oxide nanoparticles, J. Hazard. Mater. 211 (2012) 332–341.
[26] V. Nejadshafiee, M.R. Islami, Adsorption capacity of heavy metal ions using sultone-modified magnetic activated carbon as a bio-adsorbent, Mater. Sci. Eng. C 101 (2019) 42–52.
[27] M.A. Hashim, et al., Arsenic removal by adsorption on activated carbon in a rotating packed bed, J. Water Process Eng. 30 (2019), 100591.
[28] M. Asadullah, et al., Preparation of microporous activated carbon and its modification for arsenic removal from water, J. Ind. Eng. Chem. 20 (3) (2014) 887–896.
[29] M.A. Zazouli, et al., Adsorption of methylene blue from aqueous solution onto activated carbons developed from eucalyptus bark and Crataegus oxyacantha core, Water Sci. Technol. 74 (9) (2016) 2021–2035.
[30] Wang, L., K.A. Fields, and A.S. Chen, *Arsenic removal from drinking water by ion exchange and activated alumina plants*. 2000: National Risk Management Research Laboratory, Office of Research and ….
[31] N. Dutta, A. Gupta, Development of arsenic removal unit with electrocoagulation and activated alumina sorption: Field trial at rural West Bengal India, J. Water Process Eng. 49 (2022), 103013.
[32] B. Pan, et al., Acid and organic resistant nano-hydrated zirconium oxide (HZO)/polystyrene hybrid adsorbent for arsenic removal from water, Chem. Eng. J. 248 (2014) 290–296.
[33] B. Moraga, et al., Copolymer–hydrous zirconium oxide hybrid microspheres for arsenic sorption, Water Res. 166 (2019), 115044.
[34] M.R. Gandhi, S. Meenakshi, Preparation and characterization of La (III) encapsulated silica gel/chitosan composite and its metal uptake studies, J. Hazard. Mater. 203 (2012) 29–37.
[35] A. Ohki, et al., Adsorption of Inorganic and Organic Arsenic Compounds by Aluminium-loaded Coral Limestone, Appl. Organomet. Chem. 10 (9) (1996) 747–752.
[36] Z. Li, et al., As (V) and As (III) removal from water by a Ce–Ti oxide adsorbent: behavior and mechanism, Chem. Eng. J. 161 (1–2) (2010) 106–113.
[37] S. Ghosh, S. Chaudhari, Arsenic removal using electrocoagulation followed by hematite granular filter, Water Supply (2022).
[38] C.B. Tabelin, et al., Hematite-catalysed scorodite formation as a novel arsenic immobilisation strategy under ambient conditions, Chemosphere 233 (2019) 946–953.
[39] E. Di Iorio, et al., Characterization of magnetite nanoparticles synthetized from Fe (II)/nitrate solutions for arsenic removal from water, J. Environ. Chem. Eng. 7 (2) (2019), 102986.
[40] H. Basu, et al., Graphene oxide-MnO2-goethite microsphere impregnated alginate: A novel hybrid nanosorbent for As (III) and As (V) removal from groundwater, J. Water Process Eng. 42 (2021), 102129.
[41] J. López-Luna, et al., Linear and nonlinear kinetic and isotherm adsorption models for arsenic removal by manganese ferrite nanoparticles, SN Applied Sciences 1 (8) (2019) 1–19.
[42] Ü. Yenial, G. Bulut, F. Pagnanelli, Manganese ferrite nanoparticle production from industrial wastes as sorbent material for arsenic removal from aqueous solutions, Part. Sci. Technol. (2019).
[43] M.J. Uddin, Y.-K. Jeong, Application of magnesium ferrite nanomaterials for adsorptive removal of arsenic from water: Effects of Mg and Fe ratio, Chemosphere 307 (2022), 135817.
[44] K.K. Kefeni, B.B. Mamba, Photocatalytic application of spinel ferrite nanoparticles and nanocomposites in wastewater treatment, Sustain. Mater. Technol. 23 (2020) e00140.
[45] M. Jameel, et al., Structural, optical and morphological properties of zinc-doped cobalt-ferrites CoFe2− xZnxO4 (x= 0.1-0.5), Digest Journal of Nanomaterials & Biostructures (DJNB) 16 (2) (2021).
[46] K.K. Kefeni, B.B. Mamba, T.A. Msagati, Application of spinel ferrite nanoparticles in water and wastewater treatment: a review, Sep. Purif. Technol. 188 (2017) 399–422.
[47] S. Dabagh, S.A. Haris, Y.N. Ertas, Synthesis, Characterization and Potent Antibacterial Activity of Metal-Substituted Spinel Ferrite Nanoparticles, J. Clust. Sci. (2022).
[48] F. Coppola, et al., Remediation of arsenic from contaminated seawater using manganese spinel ferrite nanoparticles: Ecotoxicological evaluation in Mytilus galloprovincialis, Environ. Res. 175 (2019) 200–212.
[49] S. Martinez-Vargas, et al., Arsenic adsorption on cobalt and manganese ferrite nanoparticles, J. Mater. Sci. 52 (11) (2017) 6205–6215.
[50] W. Tang, et al., Superparamagnetic magnesium ferrite nanoadsorbent for effective arsenic (III, V) removal and easy magnetic separation, Water Res. 47 (11) (2013) 3624–3634.
[51] J. Msomi, T. Moyo, H. Abdallah, Magnetic Properties of Mg x Mn1− x Fe2O4 Nanoferrites, J. Supercond. Nov. Magn. 25 (8) (2012) 2643–2646.
[52] S. Dabagh, S.A. Haris, Y.N. Ertas, Synthesis, Characterization and Potent Antibacterial Activity of Metal-Substituted Spinel Ferrite Nanoparticles, J. Clust. Sci. (2022) 1–12.
[53] M. Kumar, H.S. Dosanjh, H. Singh, Removal of lead and copper metal ions in single and binary systems using biopolymer modified spinel ferrite, J. Environ. Chem. Eng. 6 (5) (2018) 6194–6206.
[54] J. Liu, et al., Preparation, environmental application and prospect of biochar-supported metal nanoparticles: A review, J. Hazard. Mater. 388 (2020), 122026.
[55] X. Li, et al., Efficient As (III) removal by macroporous anion exchanger-supported Fe–Mn binary oxide: behavior and mechanism, Chem. Eng. J. 193 (2012) 131–138.
[56] S. Rawat, A. Maiti, Facile preparation of iron oxyhydroxide–biopolymer (Chitosan/Alginate) beads and their comparative insights into arsenic removal, Sep. Purif. Technol. 272 (2021), 118983.
[57] S.M. Yakout, M.R. Hassan, M.I. Aly, Synthesis of magnetic alginate beads based on magnesium ferrite (MgFe2O4) nanoparticles for removal of Sr (II) from aqueous solution: kinetic, equilibrium and thermodynamic studies, Water Sci. Technol. 77 (11) (2018) 2714–2722.

[58] S. Sahu, et al., Synthesis of polypyrrole-modified layered double hydroxides for efficient removal of Cr (VI), J. Chem. Eng. Data 64 (10) (2019) 4357–4368.
[59] A. Azari, et al., Magnetic multi-walled carbon nanotubes-loaded alginate for treatment of industrial dye manufacturing effluent: adsorption modelling and process optimisation by central composite face-central design, Int. J. Environ. Anal. Chem. (2021) 1–21.
[60] M. Esmat, et al., Alginate-based nanocomposites for efficient removal of heavy metal ions, Int. J. Biol. Macromol. 102 (2017) 272–283.
[61] S. Lilhare, et al., Aloe Vera Functionalized Magnetic Nanoparticles Entrapped Ca Alginate Beads as Novel Adsorbents for Cu (II) Removal from Aqueous Solutions, Nanomaterials 12 (17) (2022) 2947.
[62] S. Martinez-Vargas, et al., As (III) and As (V) adsorption on manganese ferrite nanoparticles, J. Mol. Struct. 1154 (2018) 524–534.
[63] S. Zhang, et al., Arsenite and arsenate adsorption on coprecipitated bimetal oxide magnetic nanomaterials: MnFe2O4 and CoFe2O4, Chem. Eng. J. 158 (3) (2010) 599–607.
[64] J. Parsons, et al., Determination of arsenic (III) and arsenic (V) binding to microwave assisted hydrothermal synthetically prepared Fe3O4, Mn3O4, and MnFe2O4 nanoadsorbents, Microchem. J. 91 (1) (2009) 100–106.
[65] J. Feng, et al., Hydrothermal synthesis and characterization of Mn1− xZnxFe2O4 nanoparticles, Phys. B Condens. Matter 394 (1) (2007) 100–103.
[66] V. Rocher, et al., Removal of organic dyes by magnetic alginate beads, Water Res. 42 (4–5) (2008) 1290–1298.
[67] A. Idris, et al., Synthesis of magnetic alginate beads based on maghemite nanoparticles for Pb (II) removal in aqueous solution, J. Ind. Eng. Chem. 18 (5) (2012) 1582–1589.
[68] W.A.H. Altowayti, et al., The removal of arsenic species from aqueous solution by indigenous microbes: Batch bioadsorption and artificial neural network model, Environ. Technol. Innov. 19 (2020), 100830.
[69] S.A. Haris, et al., Arsenic biosorption using pretreated biomass of psychrotolerant Yersinia sp. strain SOM-12D3 isolated from Svalbard, *Arctic* Environmental Science and Pollution Research International 25 (28) (2018) 27959–27970.
[70] A. Sigdel, et al., Arsenic removal from aqueous solutions by adsorption onto hydrous iron oxide-impregnated alginate beads, J. Ind. Eng. Chem. 35 (2016) 277–286.
[71] S. Tsang, et al., Determination of phosphate/arsenate by a modified molybdenum blue method and reduction of arsenate by S2O42−, Talanta 71 (4) (2007) 1560–1568.
[72] K. Vijayaraghavan, et al., Biosorption of nickel (II) ions onto Sargassum wightii: application of two-parameter and three-parameter isotherm models, J. Hazard. Mater. 133 (1–3) (2006) 304–308.
[73] I. Langmuir, The adsorption of gases on plane surfaces of glass, mica and platinum, J. Am. Chem. Soc. 40 (9) (1918) 1361–1403.
[74] H. Freundlich, Over the adsorption in solution, J. Phys. chem 57 (385471) (1906) 1100–1107.
[75] R. Verma, et al., Novel glycine-functionalized magnetic nanoparticles entrapped calcium alginate beads for effective removal of lead, Microchem. J. 130 (2017) 168–178.
[76] Y.-M. Hao, C. Man, Z.-B. Hu, Effective removal of Cu (II) ions from aqueous solution by amino-functionalized magnetic nanoparticles, J. Hazard. Mater. 184 (1–3) (2010) 392–399.
[77] H.C. Vu, et al., Magnetite graphene oxide encapsulated in alginate beads for enhanced adsorption of Cr (VI) and As (V) from aqueous solutions: role of crosslinking metal cations in pH control, Chem. Eng. J. 307 (2017) 220–229.
[78] E. Manova, et al., Mechano-synthesis, characterization, and magnetic properties of nanoparticles of cobalt ferrite, CoFe2O4, Chem. Mater. 16 (26) (2004) 5689–5696.
[79] S.H. Kareem, et al., Nanostructural, morphological and magnetic studies of PEG/Mn (1–x) Zn (x) Fe2O4 nanoparticles synthesized by co-precipitation, Ceram. Int. 41 (9) (2015) 11702–11709.
[80] T. Zargar, et al., PEG coated Zn0. 3Fe2. 7O4 nanoparticles in the presence of< alpha> Fe2O3 phase synthesized by citric acid assisted hydrothermal reduction process for magnetic hyperthermia applications, Mater. Chem. Phys. 212 (2018) 432–439.
[81] R. Waldron, *Infrared spectra of ferrites.* Physical review 99 (6) (1955) 1727.
[82] S.-F. Lim, et al., Uptake of arsenate by an alginate-encapsulated magnetic sorbent: process performance and characterization of adsorption chemistry, J. Colloid Interface Sci. 333 (1) (2009) 33–39.
[83] J.P. Chen, et al., Dried waste activated sludge as biosorbents for metal removal: adsorptive characterization and prevention of organic leaching, J. Chem. Technol. Biotechnol. 77 (6) (2002) 657–662.
[84] R. Jayalakshmi, J. Jeyanthi, Synthesis and structural characterization of polymer-based cobalt ferrite nanocomposite with core–shell structure, J. Inorg. Organomet. Polym Mater. 28 (3) (2018) 1286–1293.
[85] R. Jayalakshmi, J. Jeyanthi, Dynamic modelling of Alginate-Cobalt ferrite nanocomposite for removal of binary dyes from textile effluent, J. Environ. Chem. Eng. 9 (1) (2021), 104924.
[86] M.A. Almessiere, et al., Structural, optical and magnetic properties of Tm3+ substituted cobalt spinel ferrites synthesized via sonochemical approach, Ultrason. Sonochem. 54 (2019) 1–10.
[87] A. Hajalilou, S.A. Mazlan, A review on preparation techniques for synthesis of nanocrystalline soft magnetic ferrites and investigation on the effects of microstructure features on magnetic properties, Appl. Phys. A 122 (7) (2016) 1–15.
[88] S. Mallesh, et al., Low-temperature magnetization behaviors of superparamagnetic MnZn ferrites nanoparticles, Phys. B Condens. Matter 582 (2020), 411963.
[89] M. Faham, et al., Peg decorated glycine capped mn-ferrite nanoparticles synthesized by co-precipitation method for biomedical application. Advanced Materials Research, Trans Tech Publ, 2014.
[90] M. Kumar, H.S. Dosanjh, H. Singh, Magnetic zinc ferrite–alginic biopolymer composite: as an alternative adsorbent for the removal of dyes in single and ternary dye system, J. Inorg. Organomet. Polym Mater. 28 (5) (2018) 1688–1705.
[91] M. Singh, H.S. Dosanjh, H. Singh, Surface modified spinel cobalt ferrite nanoparticles for cationic dye removal: Kinetics and thermodynamics studies, J. Water Process Eng. 11 (2016) 152–161.
[92] A. Yildirim, Y. Bulut, Adsorption behaviors of malachite green by using crosslinked chitosan/polyacrylic acid/bentonite composites with different ratios, Environ. Technol. Innov. 17 (2020), 100560.
[93] A. Ayub, et al., Development of sustainable magnetic chitosan biosorbent beads for kinetic remediation of arsenic contaminated water, Int. J. Biol. Macromol. 163 (2020) 603–617.
[94] Z. Mohd Bahari, et al., Biosorption of As (III) by non-living biomass of an arsenic-hypertolerant Bacillus cereus strain SZ2 isolated from a gold mining environment: equilibrium and kinetic study, Appl. Biochem. Biotechnol. 171 (8) (2013) 2247–2261.
[95] A.K. Meena, et al., Removal of heavy metal ions from aqueous solutions using carbon aerogel as an adsorbent, J. Hazard. Mater. 122 (1–2) (2005) 161–170.
[96] M. Podder, C. Majumder, Study of the kinetics of arsenic removal from wastewater using Bacillus arsenicus biofilms supported on a Neem leaves/MnFe2O4 composite, Ecol. Eng. 88 (2016) 195–216.
[97] R. Han, et al., Biosorption of methylene blue from aqueous solution by fallen phoenix tree's leaves, J. Hazard. Mater. 141 (1) (2007) 156–162.
[98] A. Banerjee, P. Sarkar, S. Banerjee, Application of statistical design of experiments for optimization of As (V) biosorption by immobilized bacterial biomass, Ecol. Eng. 86 (2016) 13–23.
[99] M.E. Argun, S. Dursun, M. Karatas, Removal of Cd (II), Pb (II), Cu (II) and Ni (II) from water using modified pine bark, Desalination 249 (2) (2009) 519–527.
[100] L. Wang, et al., Performance and mechanisms for remediation of Cd (II) and As (III) co-contamination by magnetic biochar-microbe biochemical composite: Competition and synergy effects, Sci. Total Environ. 750 (2021), 141672.
[101] A. Giri, R. Patel, S. Mahapatra, Artificial neural network (ANN) approach for modelling of arsenic (III) biosorption from aqueous solution by living cells of Bacillus cereus biomass, Chem. Eng. J. 178 (2011) 15–25.
[102] D. Ranjan, M. Talat, S. Hasan, Biosorption of arsenic from aqueous solution using agricultural residue 'rice polish', J. Hazard. Mater. 166 (2–3) (2009) 1050–1059.
[103] H.-Y. Chen, et al., Investigation of the toxic effect of cadmium on Candida humicola and Bacillus subtilis using a microcalorimetric method, J. Hazard. Mater. 159 (2–3) (2008) 465–470.
[104] M. Podder, C. Majumder, Removal of arsenic by a Bacillus arsenicus biofilm supported on GAC/MnFe2O4 composite, Groundw. Sustain. Dev. 1 (1–2) (2015) 105–128.
[105] J. Wang, X. Guo, Adsorption isotherm models: Classification, physical meaning, application and solving method, Chemosphere 258 (2020), 127279.
[106] L. Adlnasab, et al., Amine rich functionalized mesoporous silica for the effective removal of alizarin yellow and phenol red dyes from waste waters based on response surface methodology, Mater. Sci. Eng. B 226 (2017) 188–198.
[107] A. Sherlala, et al., Adsorption of arsenic using chitosan magnetic graphene oxide nanocomposite, J. Environ. Manage. 246 (2019) 547–556.
[108] J.A.R. Guivar, et al., Adsorption of arsenite and arsenate on binary and ternary magnetic nanocomposites with high iron oxide content, Appl. Surf. Sci. 454 (2018) 87–100.
[109] H. Basu, et al., Arsenic removal from groundwater by goethite impregnated calcium alginate beads, Water Air Soil Pollut. 226 (2) (2015) 1–11.
[110] T.M. Salem Attia, X.L. Hu, D.Q. Yin, Synthesised magnetic nanoparticles coated zeolite (MNCZ) for the removal of arsenic (As) from aqueous solution, J. Exp. Nanosci. 9 (6) (2014) 551–560.
[111] S. Lilhare, et al., Calcium Alginate Beads with Entrapped Iron Oxide Magnetic Nanoparticles Functionalized with Methionine—A Versatile Adsorbent for Arsenic Removal, Nanomaterials 11 (5) (2021) 1345.
[112] S. Kumar, et al., Graphene oxide–MnFe2O4 magnetic nanohybrids for efficient removal of lead and arsenic from water, ACS Appl. Mater. Interfaces 6 (20) (2014) 17426–17436.
[113] G. Zhang, et al., Preparation and evaluation of a novel Fe–Mn binary oxide adsorbent for effective arsenite removal, Water Res. 41 (9) (2007) 1921–1928.
[114] A.K. Mishra, S. Ramaprabhu, The role of functionalised multiwalled carbon nanotubes based supercapacitor for arsenic removal and desalination of sea water, J. Exp. Nanosci. 7 (1) (2012) 85–97.
[115] M. Podder, C. Majumder, Fixed-bed column study for As (III) and As (V) removal and recovery by bacterial cells immobilized on Sawdust/MnFe2O4 composite, Biochem. Eng. J. 105 (2016) 114–135.
[116] Y.-S. Ho, G. McKay, Pseudo-second order model for sorption processes, Process Biochem. 34 (5) (1999) 451–465.
[117] I. Oke, N. Olarinoye, S. Adewusi, Adsorption kinetics for arsenic removal from aqueous solutions by untreated powdered eggshell, Adsorption 14 (1) (2008) 73–83.
[118] S.S. Alkurdi, et al., Inorganic arsenic species removal from water using bone char: A detailed study on adsorption kinetic and isotherm models using error functions analysis, J. Hazard. Mater. 405 (2021), 124112.

[119] M. Hamayun, et al., Equilibrium and kinetics studies of arsenate adsorption by FePO4, Chemosphere 99 (2014) 207–215.
[120] P. Saha, S. Chowdhury, *Insight into adsorption thermodynamics.* Thermodynamics 16 (2011) 349–364.
[121] N.Y. Mezenner, A. Bensmaili, Kinetics and thermodynamic study of phosphate adsorption on iron hydroxide-eggshell waste, Chem. Eng. J. 147 (2–3) (2009) 87–96.
[122] R. Tabaraki, E. Heidarizadi, Simultaneous biosorption of Arsenic (III) and Arsenic (V): Application of multiple response optimizations, Ecotoxicol. Environ. Saf. 166 (2018) 35–41.
[123] S. Lata, P. Singh, S. Samadder, Regeneration of adsorbents and recovery of heavy metals: a review, Int. J. Environ. Sci. Technol. 12 (4) (2015) 1461–1478.
[124] W.H. Höll, Mechanisms of arsenic removal from water, Environ. Geochem. Health 32 (4) (2010) 287–290.
[125] V.J. Vilar, C.M. Botelho, R.A. Boaventura, Copper desorption from Gelidium algal biomass, Water Res. 41 (7) (2007) 1569–1579.
[126] M. Aryal, M. Ziagova, M. Liakopoulou-Kyriakides, Study on arsenic biosorption using Fe (III)-treated biomass of Staphylococcus xylosus, Chem. Eng. J. 162 (1) (2010) 178–185.
[127] S. Kumari, S. Mahapatra, S. Das, Ca-alginate as a support matrix for Pb (II) biosorption with immobilized biofilm associated extracellular polymeric substances of Pseudomonas aeruginosa N6P6, Chem. Eng. J. 328 (2017) 556–566.